Are your MRI contrast agents cost-effective?
Learn more about generic Gadolinium-Based Contrast Agents.
FRESENIUS KABI
caring for life

AJNR

Diffusion Tensor Microscopy Indicates the Cytoarchitectural Basis for Diffusion Anisotropy in the Human Hippocampus

T.M. Shepherd, E. Özarslan, A.T. Yachnis, M.A. King and S.J. Blackband

AJNR Am J Neuroradiol 2007, 28 (5) 958-964
http://www.ajnr.org/content/28/5/958

This information is current as of April 18, 2024.

ORIGINAL RESEARCH

T.M. Shepherd
E. Özarslan
A.T. Yachnis
M.A. King
S.J. Blackband

Diffusion Tensor Microscopy Indicates the Cytoarchitectural Basis for Diffusion Anisotropy in the Human Hippocampus

BACKGROUND AND PURPOSE: Observing changes to water diffusivity and fractional anisotropy (FA) for particular hippocampal regions may improve the sensitivity and specificity of diffusion tensor MR imaging for hippocampal pathologies like Alzheimer disease and mesial temporal sclerosis. As a first step toward this goal, this study characterized the cytoarchitectural features underlying diffusion anisotropy in human hippocampus autopsy specimens at 60-μm in-plane resolution.

MATERIALS AND METHODS: Eight-millimeter coronal segments of the hippocampal body were dissected from 5 autopsy specimens (mean = 55.6 ± 6.2 years of age) with short postmortem intervals to fixation (21.2 ± 5.7 hours) and no histologic evidence of neuropathology. Diffusion tensor microscopy data were collected from hippocampal specimens by using a 14.1T magnet with a protocol that included 21 unique diffusion gradient orientations (diffusion time = 17 ms, b = 1250 s/mm^2). The resulting images were used to determine the mean diffusivity, FA, and principal fiber orientation for manually segmented hippocampal regions that included the stratum oriens, stratum radiatum, stratum pyramidale (CA1 and CA3), stratum lacunosum-moleculare, hilus, molecular layer, granule cell layer, fimbria, and subiculum.

RESULTS: Diffusion-weighted images had high signal-to-noise ratios (31.1 ± 13.0) and delineated hippocampal anatomy well. Water diffusivity ranged from $1.21 \pm 0.22 \times 10^{-4}$ mm^2/s in the fimbria to $3.48 \pm 0.72 \times 10^{-4}$ mm^2/s in granule cells (analysis of variance, $P < .001$). Color fiber-orientation maps indicated the underlying microstructures responsible for diffusion anisotropy in the hippocampal lamina.

CONCLUSION: Diffusion tensor microscopy provided novel microstructural information about the different lamina of the human hippocampus. These ex vivo data obtained at high-magnetic-field strengths can be used to study injury-specific diffusion changes to susceptible hippocampal regions and may lead to more specific MR imaging surrogate markers for Alzheimer disease or epilepsy.

The hippocampus, a critical structure for learning and semantic memory formation,[1] is susceptible to a wide variety of neurologic diseases, including hypoxia-ischemia, epilepsy, Alzheimer disease, or schizophrenia.[2] The consequences of hippocampal disease can be devastating.[3] MR imaging is commonly used for the diagnosis, prognosis, and monitoring of hippocampal disease processes. Yet, the hippocampus is a small complicated multilaminar structure, which is challenging to image in detail with current clinical MR imaging scanners. Thus, for example, clinical studies have often described MR imaging–defined volume changes to the whole hippocampus; however, these findings can be seen in many diseases.[4-6] Without adequate image resolution or more specific tissue-contrast methods, MR imaging studies are unable to discriminate the pathologic changes to anatomic regions of the hippocampus that are known to be selectively vulnerable to particular diseases (eg, granule cell dispersion and mossy fiber sprouting in hippocampal sclerosis)[7]; this shortcoming limits the sensitivity and specificity of MR imaging methods as surrogate markers of hippocampal injury.

Recent studies have shown that the laminar anatomy of the hippocampus is resolved well in MR imaging by using high-magnetic-field strengths that may become practical for in vivo imaging in a few years.[8-9] For example, this approach can be used to characterize specific changes to CA1 and subicular components of the hippocampus that may correlate with the severity of Alzheimer disease.[10] Along with higher resolutions, diffusion tensor MR imaging,[11-12] which characterizes how water diffusion in nervous tissue is influenced by the 3D coherent orientation of microstructures,[13] may improve imaging of the hippocampus in diseases like epilepsy or schizophrenia.[14-16] This study presents a combination of diffusion tensor methods with microscopy acquisitions capable of distinguishing particular hippocampal lamina that are selectively vulnerable to different disease processes. This combination is referred to as diffusion tensor microscopy (DTM). To first increase our understanding of the relationship between tissue cytoarchitecture and water diffusion anisotropy in the different laminar regions of the unaffected hippocampus, we characterized healthy human hippocampus autopsy specimens with DTM at 60-μm in-plane resolution by using a 14.1T magnet. Although such images are impractical to acquire with current clinical MR imaging scanners, the results of this ex vivo study may help interpret diffusion changes that accompany injury to this important structure.

Received April 27, 2006; accepted after revision August 21.

From the Department of Neuroscience (T.M.S., M.A.K., S.J.B.), McKnight Brain Institute, University of Florida, Gainesville, Fla; the Departments of Computer and Information Science and Engineering (E.Ö) and Pathology (A.T.Y.), University of Florida, Gainesville, Fla; the NF/SG Veterans Health Center (M.A.K.), Gainesville, Fla; and the National High Magnetic Field Laboratory (S.J.B.), Tallahassee, Fla.

This work was supported by grant sponsors: NIH R01 NS36992 and P41 RR16105.

Paper previously presented at the Annual Meeting of the American Society of Neuroradiology, May 21–27, 2005; Toronto, ON, Canada.

Please address correspondence to Timothy Shepherd, MD, PhD, Department of Internal Medicine, University of Florida, 655-1 West 8th St, Jacksonville, FL 32209; e-mail: tms@mbi.ufl.edu

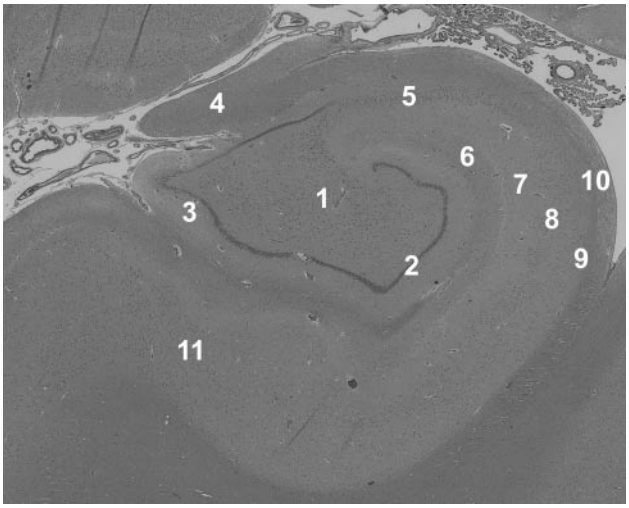

Fig 1. Histology demonstrates the laminar anatomy of the human hippocampus. This section was taken adjacent to one of the autopsy samples imaged in this study—no evidence of pathology was seen in any of the tissue samples. 1 indicates hilus; 2, granule cell layer; 3, molecular layer; 4, fimbria; 5, CA3 stratum pyramidale; 6, stratum lacunosum-moleculare; 7, stratum radiatum; 8, CA1 stratum pyramidale; 9, stratum oriens; 10, alveus; 11, subiculum (hematoxylin-eosin, original magnification ×4).

Methods

Hippocampal Tissue Procurement

The use of tissue from human brain autopsy specimens was approved by the University of Florida Institutional Review Board. During autopsy, the brain was carefully removed and suspended in 20% formalin (pH 7.4). After 7–10 days of immersion fixation, the brain was washed in distilled water for 12 hours, then sliced into 1-cm-thick coronal sections per standard practice. Following gross pathologic assessment, samples of the hippocampal body at the level of the lateral geniculate nucleus were dissected carefully from the coronal brain section to include the hippocampus proper, dentate gyrus, fimbria, and subiculum. Samples were re-immersed in 4% formaldehyde in phosphate-buffered saline (300 mOsm/kg, pH 7.4) for storage at 4°C until needed for the DTM experiments. Hippocampal autopsy samples with postmortem intervals greater than 24 hours, significant clinical history of neurologic disease, or obvious hippocampal pathology during gross examination were not collected for further study. Sections adjacent to the MR imaging samples were sent for standard histologic examination (Fig 1). A neuropathologist (A.T.Y.) analyzed these sections for evidence of pathology—samples with documented neuropathology in the final autopsy report (eg, agonal hypoxic-ischemic changes to the CA1 region) were excluded from the study.

DTM of Human Hippocampus Samples

Before DTM data collection, the hippocampal samples were warmed gradually to room temperature, then washed in phosphate-buffered saline 5–6 times during 24 hours to remove free formaldehyde, which causes significant T2 shortening effects in nervous tissue.[17] The coronally oriented hippocampal samples then were pushed into the bottom of a 10-mm-diameter nuclear magnetic resonance tube with a polished glass rod such that the in vivo medial-to-lateral axis of the hippocampus was collinear with the long axis of the tube. Typically, the hippocampi were approximately 18 × 8 × 8 mm so that the samples fit snugly inside the tube (inner diameter ~ 9 mm). The samples were immersed in Fluorinert (3M, St Paul, Minn) to eliminate extraneous signal intensity from protons outside the tissue. The samples were placed into a 10-mm Helmholtz pair coil inside a 14.1T magnet with 3000 mT/m gradients. Multisection sagittal, coronal, and axial pilot T1-weighted images were used to define MR imaging sections through the hippocampal samples that mimicked coronally oriented images of the in vivo hippocampus.

DTM data were obtained at room temperature with a multisection pulsed gradient spin-echo sequence (TR/TE = 1500/34 ms, bandwidth = 35 kHz). First, an image without diffusion-weighting was collected, then 21 diffusion-weighted images were collected with a 415 mT/m diffusion gradient (T_d = 17 ms, δ = 2.4 ms, b = 1250 s/mm^2). To extract the anisotropy of water diffusion, each of these images used a diffusion gradient applied along a different direction. Gradient orientations were obtained from the 1st-order tessellations of an icosahedron on the unit hemisphere. The image-acquisition geometry typically had 15–25 contiguous 300-μm-thick sections. The field-of-view was 9.6-mm wide and 16–21 mm in length (depending on the particular sample)—matrix size in the frequency axis then varied by sample length, but the phase-encoding axis always had 160 steps to generate 60-μm in-plane image resolution. The image without diffusion-weighting had 36 signal-intensity averages (time = 2.4 hours), and the diffusion-weighted images each had 12 averages (time = 0.8 hours) to give a total imaging time of 19.2 hours per sample.

Diffusion Tensor Microscopy Data Analysis

The apparent diffusion tensor at each image voxel was fitted to the resulting MR imaging data and used to calculate an image without diffusion-weighting (S0) as well as maps of mean diffusivity (MD), fractional anisotropy (FA), and color fiber orientation for the hippocampi.[11,12] Different regions of interest in the hippocampus were manually segmented by using the non-diffusion-weighted images (S_0) with custom-built computer software (Fig 2). These regions of interest were identified on the basis of anatomic literature[1] and histology of the hippocampus (Fig 1) and included the stratum oriens, the stratum pyramidale (CA1 and CA3), the stratum radiatum, and the stratum lacunosum-moleculare in the hippocampus proper; the hilus, molecular, and granule cell layers of the dentate gyrus; as well as the fimbria and subiculum. Quantitative data from the FA and MD maps were obtained by using these regions of interest.

Both FA and MD values for different cytoarchitectural regions of the hippocampi were compared with a 1-way analysis of variance (ANOVA) and a Tukey multiple comparisons test (SigmaStat for Windows, version 2.03, SPSS, San Rafael, Calif). Significance for all statistical tests was predetermined at $P < .05$. Signal-to-noise ratios (SNR) were calculated for several diffusion-weighted images from each sample as the mean signal intensity in the hippocampus (minus the mean noise signal intensity) divided by the SD of the noise signal intensity.

Results

Before DTM data acquisition, tissue sections adjacent to the hippocampal samples were examined by a neuropathologist (Fig 1) for signs of pathology such as hypoxic-ischemic changes. The laminar anatomy of the hippocampus evident in Fig 1 was well demonstrated in the subsequent DTM data obtained, and the stained histology sections confirmed the image segmentations. Samples were excluded from the study for postmortem intervals greater than 24 hours ($n = 4$), inability to determine the postmortem interval ($n = 2$), or histopathologic evidence of hypoxic-ischemic changes in the hippocampus ($n = 5$). Ultimately, 5 of the original 16 autopsy samples collected at gross dissection during a 6-month period in 2004 were included for this study. These

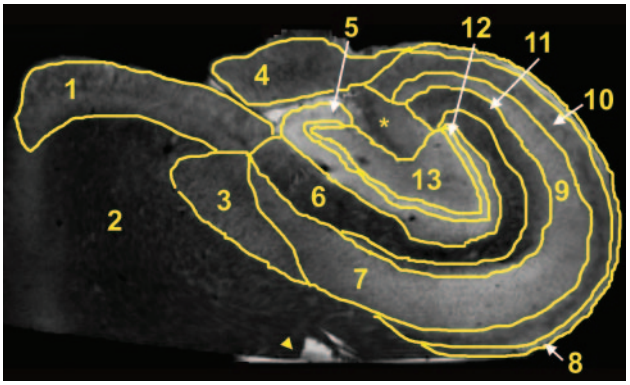

Fig 2. Manually segmented regions of interest on a non-diffusion-weighted image of a human hippocampus. These regions include the subiculum (1), the parahippocampal white matter (2), the presubiculum (3), the fimbria (4), the molecular layer (5), the stratum lacunosum-moleculare (6), the CA1 stratum pyramidale (7), the alveus (8), the CA3 stratum pyramidale (9), the stratum oriens (10), the stratum radiatum (11), the granule cell layer (12), and the hilus (13). The asterisk indicates a hippocampal area that could not be assigned unambiguously. The arrowhead indicates some water on the free surface of this particular sample that was not removed by immersion in Fluorinert.

samples were obtained from 3 male and 2 female patients who had a mean age of 55.6 ± 6.2 years, a mean postmortem interval of 21.2 ± 5.7 hours, and various non-neurologic causes of death. No signs of pathology or autolytic changes secondary to the postmortem interval were evident in any of the histologic sections obtained (Fig 1). Although not recorded, the portion of the postmortem interval before cadaver refrigeration was estimated to be less than 4 hours for all samples. No obvious differences for the sample with a shorter postmortem interval of 11 hours were noted in the histology or subsequent DTM analysis—again, probably because tissue samples spent most of the postmortem interval in refrigeration, thus retarding any autolytic processes that may alter the MR imaging properties of the sample.

Simple diffusion-weighted images resolved the internal layers of the hippocampus (Fig 3). There was no evidence of gross morphologic damage or distortion to any of the samples in the diffusion MR imaging data. Although all 5 samples were coronal sections from the hippocampal body, the cytoarchitectural regions of the hippocampi varied slightly in size and shape in the different samples (Fig 3). SNRs for the hippocampi in the diffusion-weighted images were 31.0 ± 13.0 at b = 1250 s/mm^2 (n = 5). Diffusion tensor datasets were calculated from these images (Fig 4), then used to generate parameter maps of no diffusion-weighting (S_0), MD, and FA (Fig 5). Non-diffusion-weighted images demonstrated enough detail for region-of-interest segmentation of the different regions (Fig 2). Contrast in these non-diffusion-weighted images suggested that there were some T2 and proton density differences between the hippocampal regions (Figs 2 and 5).

Mean diffusivity images (Fig 5) demonstrated similar contrast relationships to the simple diffusion-weighted images (Fig 3) but also accounted for the potentially confounding effects of diffusion anisotropy, proton density, and T2 differences. For example, diffusion appeared slow for CA1 and CA3 in the diffusion-weighted images (Fig 3) because of the particular gradient orientations, yet the mean diffusivities for these regions were actually high (Fig 5). Mean water diffusivities were lowest in regions of white matter or predominately axonal architectures (fimbria, alveus, and stratum oriens) and highest in layers composed of neuronal cell bodies (stratum granulosum, CA3 stratum pyramidale, and subiculum). A 3rd group with mixed architecture composed of neuronal cell bodies and neuropil (hilus, molecular layer, and stratum radiatum) appeared to have intermediate diffusivities. MDs for some of the different laminar regions of the rat hippocampus were statistically different despite the limited number of samples (Fig 6) (ANOVA, $P < .05$).

FA maps also demonstrated several fine anatomic details and laminar divisions of the rat hippocampus (Fig 5). Similar to diffusivity, the FA values reflected differences between subregions dominated by particular cytoarchitectural features (Fig 6) (ANOVA, $P < .05$). FA was highest in regions of known white matter or densely packed coherent axonal projections (fimbria, stratum oriens, alveus, parahippocampal gyrus, and stratum lacunosum-moleculare), whereas lower FA was noted where neuronal perikarya were concentrated (stratum pyramidale of CA1 and CA3, stratum granulosum, and subiculum). Intermediate FA values were noted in the stratum radiatum, hilus, and presubiculum. There appeared to be an inverse relationship between FA and diffusivity in the hippocampus (Fig 5), such that regions with high diffusivity correlated with regions of low anisotropy and vice versa, but there were exceptions (parahippocampal gyrus white matter and CA1). What is most interesting, the FA map suggested that the molecular layer could be divided into inner and outer layers, with the former having higher FA. Color fiber-orientation maps (Fig 7) based on the principal eigenvector from the diffusion tensor data provided exceptional anatomic contrast for the different hippocampal layers. The interpretation of these findings will be discussed in much detail below.

Discussion

Diffusivity and FA of the Hippocampus

The laminar anatomy of the hippocampus found within conventional postmortem histologic preparations of the hippocampus (Fig 1) was well demonstrated in simple diffusion-weighted images (Fig 3) and in MD and FA images derived from the diffusion tensor analysis (Fig 5). To improve the value of MR imaging as a surrogate marker of hippocampal injury, one should note that high spatial resolution is not alone sufficient, but adequate contrast is also required to observe changes to specific hippocampal lamina. Diffusivity and FA provided adequate contrasts between hippocampal layers for this purpose. This work demonstrated some statistically significant differences in water diffusion for various regions of human nervous tissue (Figs 5 and 6). Similar diffusion differences were reported in viable unfixed rat hippocampal sections by using both diffusion MR imaging[18] and tetramethyl ammonium iontophoresis.[19] This suggests that the observed relative differences in water diffusion for different hippocampal lamina are likely valid for unfixed hippocampus in vivo.

Differences in water diffusivity may best be explained by the improved spatial resolution of hippocampal layers in this DTM study. Unlike the isocortex, the phylogenetically older hippocampus contains segregated cytoarchitectural regions where volumes are dominated by large neuronal somata (eg, stratum pyramidale), neuropil (eg, stratum lacunosum-moleculare), or a mixture of the 2 (eg, hilus). The MD of water in nervous tissue ap-

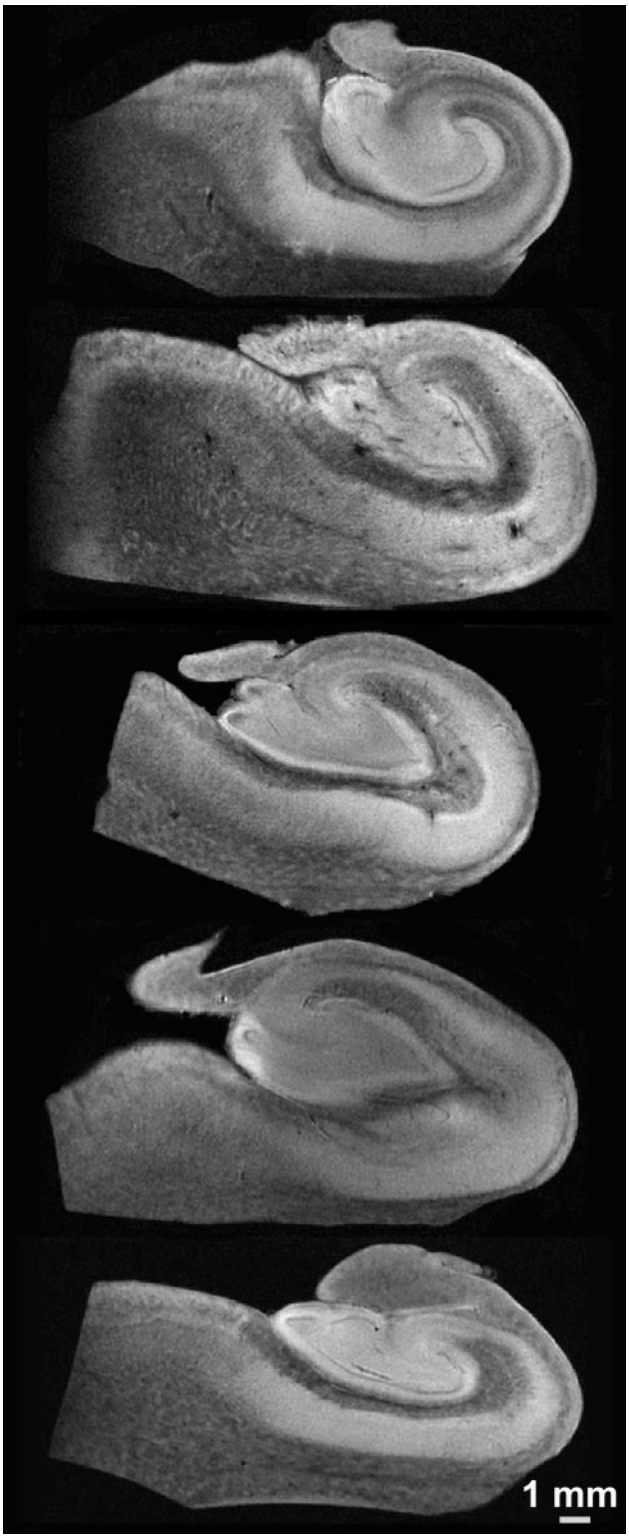

Fig 3. Representative 60-μm in-plane resolution diffusion-weighted images (b $\sim$ 1250 s/mm^2) from each of the 5 human hippocampus autopsy specimens. Random diffusion gradient orientations (from the 21 directions acquired for each sample) are shown. The laminar anatomy of the hippocampal body is well resolved.

pears to decrease significantly as the tissue cytoarchitecture becomes volume-dominated by microscopic tubular structures such as axons and dendrites. The diffusion of water is most restricted in regions with relatively homogeneous collections of coherent, myelinated axon bundles such as the fimbria. Conversely, regions of large densely packed pyramidal or spheric-shaped neuronal soma (ie, stratum granulosum) have high mean water diffusivities. Intermediate values occur in neuropil, where there are complex microscopic interdigitations of axons, dendrites, and dendritic spines, such as the stratum radiatum.

The values observed for diffusion anisotropy in the human hippocampus are lower than those reported for white matter tracts like the corpus callosum.[20] Specific interpretations of the structures underlying FA in the different hippocampal lamina are discussed in the context of fiber orientation. At the image resolutions obtained, the fiber architecture in the hippocampus is more complex than that in traditional white matter so that many regions may contain an intravoxel volume averaging of multiple orientations. For example, the stratum lucidum contains mossy fibers from granule cells in the dentate gyrus crossing the orthogonally oriented apical dendrites of CA3 pyramidal neurons.[21] These 2 "fibers" in fact synapse to one another en passage and represent part of the trisynaptic pathway. Although there is significant coherence to these 2 underlying fiber architectures within the stratum lucidum, the diffusion tensor may underestimate the FA of nonmonopolar coherences because the tensor model gives rise to excessive smoothing in regions of orientation heterogeneity.[22,23] The divergence of axonal projections and dendritic arbors also may reduce coherence variably. Similar effects may be observed in other regions that contain 2 or more crossing-fiber coherences, such as the hilus, stratum radiatum, stratum lacunosum-moleculare, and stratum oriens so that FA values will be reduced. In this study, the protocol for measuring diffusion anisotropy was kept similar to methods currently used clinically. However, in future studies, alternative more data-intensive methods of measuring diffusion anisotropy,[24,25] which may indicate crossing-fiber coherences, could improve the characterization of these regions. The FA of the hippocampus also may appear lower than that of the anisotropic brain structures like the corpus callosum because of higher SNR in the present data[26] and/or the effects of chemical fixation on the tissue.[17] Preliminary studies in rat spinal cord white matter also suggest that FA decreases 30% during a 24-hour postmortem interval when prefixed tissue was kept at room temperature,[27] though autopsy samples here were refrigerated before fixation to mitigate this effect.

Hippocampal Cytoarchitecture as the Basis for Fiber Orientation

The orientation of cytoarchitecture indicated in the color fiber-orientation maps for different hippocampal lamina (see selected example in Fig 7) can best be interpreted on the basis of components of the trisynaptic intrahippocampal pathway involved in semantic memory formation.[1] For instance, high anisotropy in the fimbria can be attributed to efferent axons from CA3, CA1, and the subiculum, along with afferent axons from the septal regions of the brain—these fibers run parallel to the septal-temporal axis of the hippocampus. Similarly, the thin alveus contains the efferent hippocampal axon fibers as they exit from the CA1 and subicular regions to wrap around the surface of the hippocampus in an oblique septal direction toward the fimbria and subsequently the fornix. The stratum oriens first contains these axons after they exit the CA1 and CA3 neuronal layers and bend into the alveus. It also contains basal dendrite arborizations from pyramidal neurons that will be oriented orthogonal to the exiting axons and apical den-

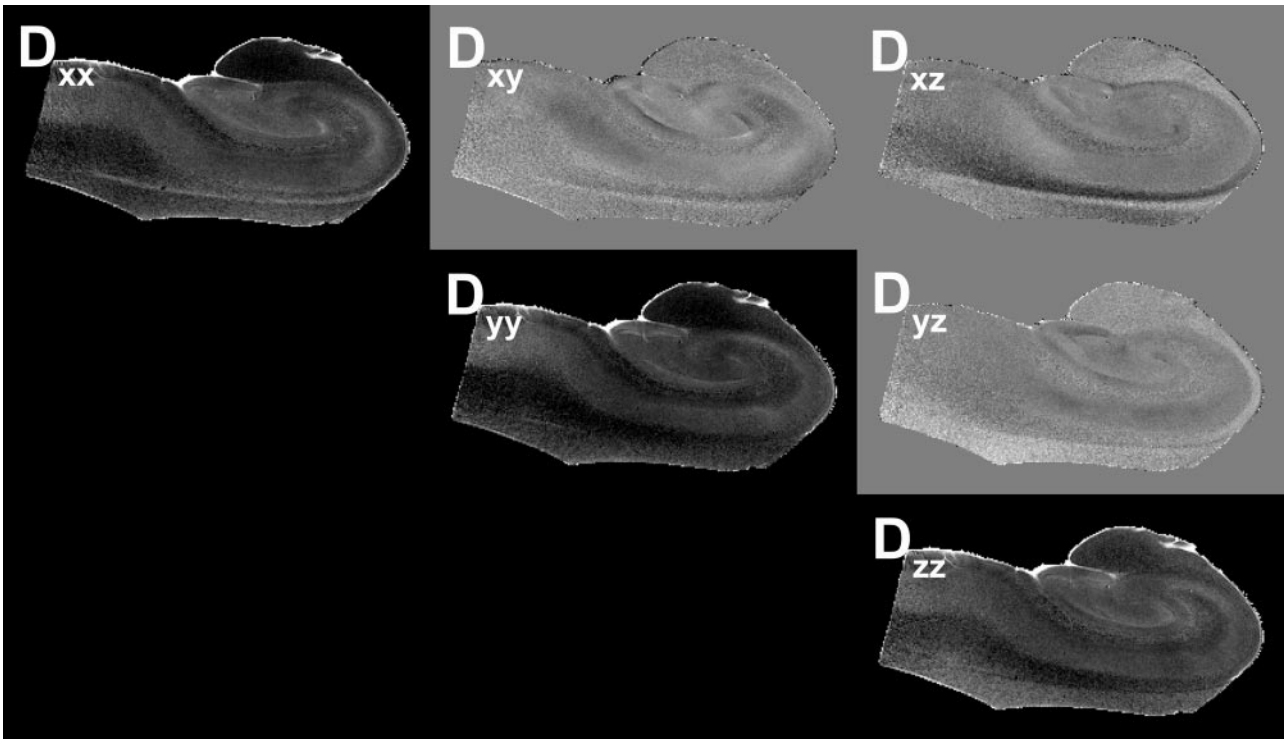

Fig 4. Images of the components of the diffusion tensor visualized on a section from one of the human hippocampus autopsy specimens. The diagonal elements of the tensor (D_{xx}, D_{yy}, D_{zz}) depict the water mobility along the 3 orthogonal directions, x, y, and z, respectively. The apparent differences between the images obtained from these diagonal elements are due to the anisotropy of water diffusion inside the sample, where the higher intensity voxels correspond to regions with higher (or less restricted) diffusion. These images are scaled between the values of zero and 8×10^{-4} mm^2/s. The off-diagonal elements (D_{xy}, D_{xz}, D_{yz}) indicate the correlations of diffusional motion along 2 orthogonal directions. Because the off-diagonal elements can take negative values, these images are scaled between -2×10^{-4} and 2×10^{-4} mm^2/s—hence the gray background.

drites of pyramidal neurons. These 2 features may explain the blue transverse fiber orientation of this lamina in Fig 7.

In the stratum pyramidale underlying the stratum oriens, CA3 tends to have slightly higher FA and appears thinner than the CA1 pyramidal neuron layer. The latter can be predicted on the basis of neuronal packing density differences observed in routine histology of the hippocampus (Fig 1). In the fiber-orientation map (Fig 7), it is difficult to distinguish a clear border between the stratum pyramidale and the stratum radiatum. The radial fiber orientations observed for the stratum pyramidale and radiatum can best be attributed to the large apical dendrites of CA1 and CA3 pyramidal neurons projecting through these layers toward their termination in the stratum lacunosum-moleculare. The region of the stratum pyramidale adjacent to the stratum radiatum will already contain many of these apical dendrites projecting from more basally located pyramidal neurons, thus explaining the blending of these 2 layers as well as the increasing FA as one moves away from the relatively isotropic border with the stratum oriens. This thin band of isotropy may reflect the basal portion of the stratum pyramidale (the stratum profundum), where the relatively isotropic pyramidal neuron cell bodies are packed with minimal intravoxel contributions from apical dendrites. The stratum lacunosum-moleculare may be less anisotropic than the stratum radiatum because the apical dendrites diverge orthogonally into terminal arborizations that tend to run parallel to the hippocampal sulcus rather than along the apical axis. Fiber orientation here also appears affected by Schaffer collaterals from CA3 and perforant fibers that project into these layers orthogonal to the pyramidal neuron apical dendrites.

A thin isotropic line representing the residual hippocampal sulcus separates the hippocampus proper from the dentate gyrus. The fiber orientation of the molecular layer in the dentate gyrus appears dominated by the radial extensions of granule cell dendrites into the molecular layer (Fig 7). Of note, FA divided the molecular layer—higher FA was observed for the inner half, and lower FA, for the outer half (Figs 5 and 7). This division may relate to the magnitude and orientation of intravoxel contributions from commissural/septal fibers in the inner molecular layer and the perforant pathway fibers in the outer molecular layer versus the dominant granule cell dendrite orientation. Anisotropy in the stratum granulosum can be explained similarly to that in the CA1 and CA3 neuron layers—dendrites from the most basal granule cells in this lamina will extend through the densely packed more superficial granule cells en route to the molecular layer and increase the FA of the granule cell layer adjacent to the molecular layer. Also, like the CA3 region, the basal aspects of the granule cell layer are isotropic because of the preponderance of densely packed granule cells with minimal dendrites. This renders this part of the granule cell layer indistinguishable from the underlying isotropic polymorphic layer in the fiber-orientation map. Deep to these layers, the hilus appears to demonstrate a funneling of axons projecting from the internal and external blades of the dentate gyrus as the mossy fiber afferents to CA3 neurons. Furthermore, the stratum lucidum terminal field appeared as a blue region of fiber orientation on either side of the distal CA3 pyramidal neurons (Fig 7). These regions likely represent the en passage connections between mossy fibers and the dendrites of CA3 neurons.

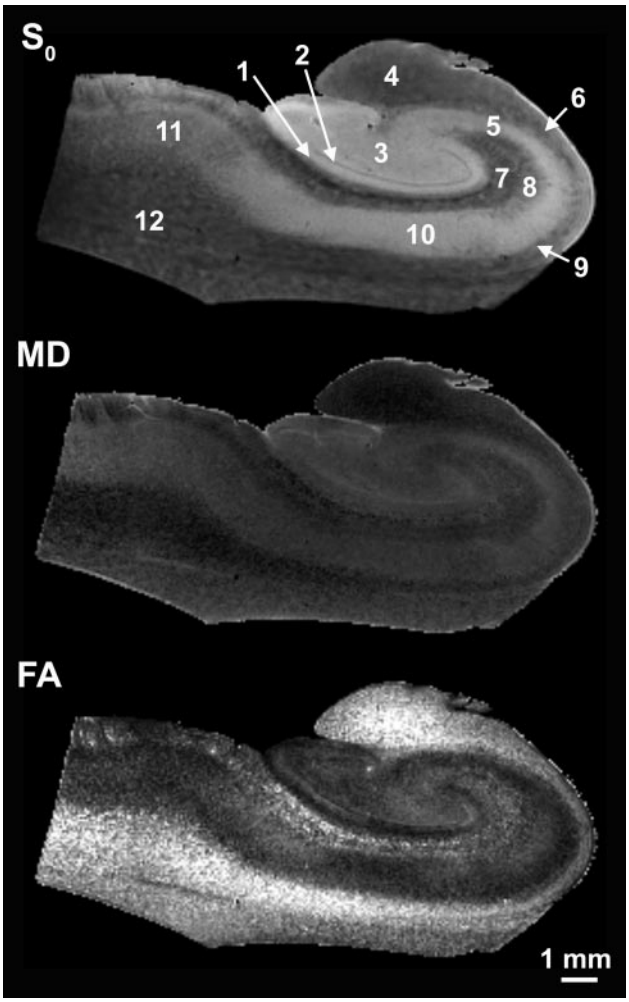

Fig 5. Sixty-micrometer in-plane resolution images of no diffusion-weighting (S_0), MD, and FA in the human hippocampus. In the S0 image, the layers of the hippocampus have different T2s and proton densities. In the MD image, water diffusion appeared highest (light) in regions of densely packed cells and lowest (dark) in coherent white matter such as the fimbria. Intermediate diffusivity was observed in the hilus, stratum radiatum, or subiculum. FA demonstrates excellent resolution of the hippocampal lamina. Diffusion anisotropy is highest in the fimbria, stratum oriens, alveus, and white matter from the parahippocampal gyrus. Anisotropy is lowest in the pyramidal and granule cell layers. Note also the division of the molecular layer into inner and outer layers on the basis of FA differences. 1 indicates molecular layer; 2, granule cell layer; 3, hilus; 4, fimbria; 5, CA3 stratum pyramidale; 6, alveus; 7, stratum lacunosum-moleculare; 8, stratum radiatum; 9, stratum oriens; 10, CA1 stratum pyramidale; 11, subiculum; 12, white matter.

Additional structures of interest in these samples included the subiculum and underlying white matter of the parahippocampal gyrus. Contrasts in the color fiber-orientation map are particularly striking for separating the subiculum from the adjacent CA1 subregion—the anisotropic subiculum and the anisotropic wedge-shaped termination of CA1 are separated by a relatively isotropic region that is sometimes referred to as the presubiculum (Fig 7).[2] The subiculum itself was similar to the stratum radiatum in that it had radial fiber orientations orthogonal to its surface from the dendrites and exiting axons of subicular neurons.

Diffusion Tensor Microscopy of Human Autopsy Tissue

This DTM study benefited from using postmortem human hippocampal tissue chemically fixed in formaldehyde solutions. This approach significantly improved achievable SNR by allowing longer MR imaging times without subject motion or pulsation artifacts and by the dissected isolation of the hippocampus to reduce radio-frequency coil size and use a very high-field narrow-bore research magnet. This approach also enabled correlative histology from imaged samples when desired. Several practical issues, however, have limited the use of diffusion tensor microscopy in current MR imaging research. Tissue samples may be detrimentally affected during the "postmortem interval" by autolysis that occurs during lengthy delays to tissue refrigeration, dissection, and chemical fixation following a patient's death.[28] Obtaining hippocampal tissue also can be difficult because the number of autopsies (especially those that include brain dissection) has decreased significantly in the United States.[29] This decrease is particularly true for patients without significant disease comorbidities. In this study, only about 10% of the brains dissected for autopsy over a 6-month period from our institution provided acceptable hippocampal tissue—many tissue samples were rejected because of excessive postmortem intervals (> 24 hours) or evidence of significant neuropathology.

Furthermore, the effects of chemical fixatives, such as 4% formaldehyde, on MR imaging contrast mechanisms remain an area of active inquiry. Some reports suggest that nervous tissue fiber orientations observed by diffusion tensor MR imaging were not changed by chemical fixation,[30] but other studies have demonstrated that the restrictive effects of cellular membranes were altered by the commonly used aldehyde fixatives so that relative differences in diffusion anisotropy and the in vivo fiber orientations may be preserved but the absolute values for FA and water diffusivity may differ between in vivo and ex vivo fixed samples.[17] Clearly, additional fundamental research into these practical but important issues will be required to increase our confidence in extrapolating DTM data obtained from chemically fixed tissue to in vivo studies. Human brain tissue banks also may help alleviate the problems associated with obtaining high-quality nervous tissue with short postmortem intervals for MR imaging research.

Conclusion

By using autopsy specimens, this diffusion tensor microscopy study characterized the cytoarchitectural features underlying water diffusion anisotropy in the human hippocampus. Water diffusion in the different lamina of the hippocampus was found to be significantly different. FA also varied in a region-dependent manner and was highest in traditional white matter structures like the fimbria, whereas moderate levels of anisotropy were detected in neuropil layers of the hippocampus like the stratum radiatum. Fiber-orientation maps demonstrated excellent contrast resolution of the hippocampal layers and could be interpreted by using cytoarchitectural features from the different components of the trisynaptic pathway. These data may be amenable to diffusion anisotropy–based tractography investigations of the interneuronal connectivity in the hippocampus and how it is altered by different hippocampal diseases.

In the future, these methods could be applied to diseased hippocampi obtained from autopsy samples or surgical biopsy samples to better characterize MR imaging changes in particular regions of the hippocampus that are selectively vulnerable to particular disease processes, such as the mossy fibers and the granule cell layer in epilepsy.[7] Alternative methods of measuring diffusion anisotropy, such as the diffusion orientation

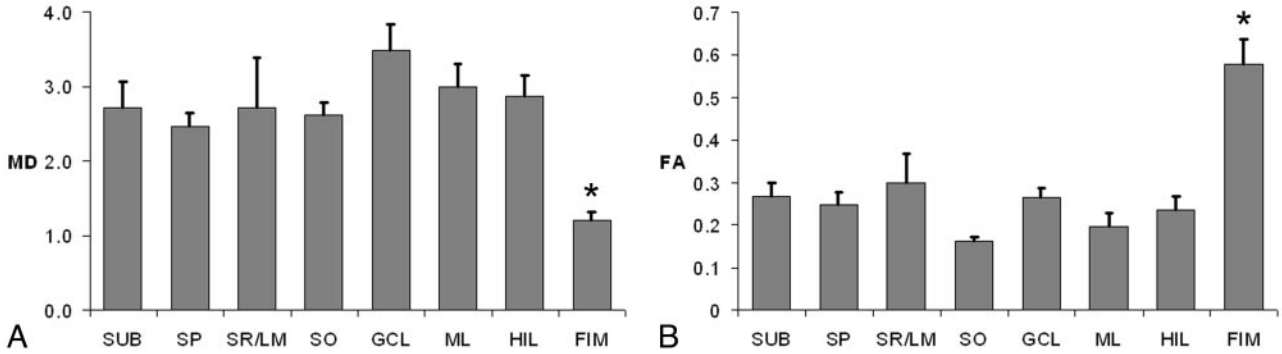

Fig 6. Comparison of MD ($\times 10^{-4}$ mm^2/s) (*A*) and FA (no units) (*B*) for the different regions of the hippocampus (Mean ± standard error of the mean, 5 hippocampi). The MD and FA of the fimbria (asterisk) are statistically different from all other regions (Tukey multiple comparisons tests, $P < .01$). SUB indicates subiculum; SP, stratum pyramidale; SR/LM, stratum radiatum lacunosum-moleculare; SO, stratum oriens; GCL, granule cell layer; ML, molecular layer; HIL, hilus; FIM, fimbria.

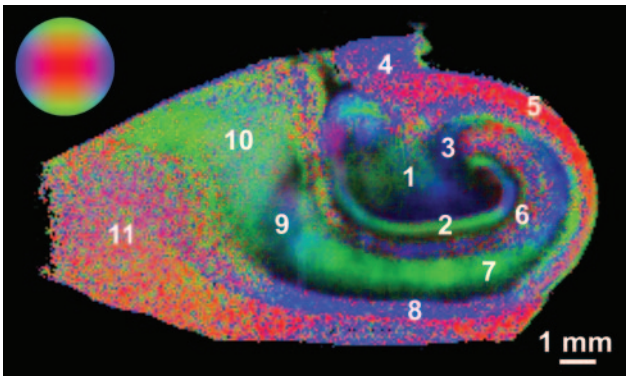

Fig 7. Color fiber-orientation maps of the human hippocampus derived from diffusion tensor microscopy data provide excellent contrast resolution for the different layers of the hippocampus. Color intensity is proportional to the FA within that pixel. The colorball indicates the direction of the principal eigenvector, which can be transverse (blue), vertical (green), or through the plane of the image (red). 1 indicates hilus; 2 , molecular layer; 3, stratum lucidum; 4, fimbria; 5, alveus, 6; stratum lacunosum-moleculare; 7, stratum radiatum/pyramidale; 8, stratum oriens; 9, presubiculum; 10, subiculum; 11, white matter.

transform,[25] may improve our understanding of complex cytoarchitecture in certain hippocampal regions like the hilus. These methods could provide more accurate estimates of diffusion anisotropy and depict multiple coherent fiber pathways within particular regions of the hippocampus. Ultimately diffusion tensor microscopy of autopsy samples at high-magnetic-field strengths may improve our understanding of the relationship between selective vulnerability in particular regions of the hippocampus and the water diffusion changes noted in clinical MR imaging of patients with hippocampal disease.

Acknowledgments

We thank the patients and their families for the tissue donations that made these experiments possible. We also appreciate technical assistance from Dan Plant.

References

1. Duvernoy HM. *The Human Hippocampus.* New York: Springer-Verlag; 1998:39–72
2. Insausti R, Amaral DG. Hippocampal formation. In: Paxinos G, Mai JK, eds. *The Human Nervous System.* 2nd ed. Boston: Elsevier Academic Press; 2004: 871–914
3. Larson EB, Kukull WA, Katzman RL. **Cognitive impairment: dementia and Alzheimer's disease.** *Annu Rev Public Health* 1992;13:431–49
4. Van Paesschen W. **Qualitative and quantitative imaging of the hippocampus in mesial temporal lobe epilepsy with hippocampal sclerosis.** *Neuroimaging Clin N Am* 2004;14:373–400
5. Sheline YI, Wang PW, Gado MH, et al. **Hippocampal atrophy in recurrent major depression.** *Proc Natl Acad Sci U S A* 1996;93:3908–13
6. Bigler ED, Blatter DD, Anderson CV, et al. **Hippocampal volume in normal aging and traumatic brain injury.** *AJNR Am J Neuroradiol* 1997;18:11–23
7. Sutula T, Cascino G, Cavazos J, et al. **Mossy fiber synaptic reorganization in the epileptic human temporal lobe.** *Ann Neurol* 1989;26:321–30
8. Fatterpekar GM, Naidich TP, Delman BN, et al. **Cytoarchitecture of the human cerebral cortex: MR microscopy of excised specimens at 9.4 Tesla.** *AJNR Am J Neuroradiol* 2002;23:1313–21
9. Chakeres DW, Whitaker CD, Dashner RA, et al. **High-resolution 8 Tesla imaging of the formalin-fixed normal human hippocampus.** *Clin Anat* 2005;18:88–91
10. Adachi M, Kawakatsu S, Hosoya T, et al. **Morphology of the inner structure of the hippocampal formation in Alzheimer disease.** *AJNR Am J Neuroradiol* 2003;24:1575–81
11. Basser PJ. **Inferring microstructural features and the physiological state of tissues from diffusion-weighted images.** *NMR Biomed* 1995;8:333–44
12. Basser PJ, Mattiello J, LeBihan D. **Estimation of the effective self-diffusion tensor from the NMR spin echo.** *J Magn Reson B* 1994;103:247–54
13. Beaulieu C. **The basis of anisotropic water diffusion in the nervous system: a technical review.** *NMR Biomed* 2002;15:435–55
14. Wieshmann UC, Clark CA, Symms MR, et al. **Water diffusion in the human hippocampus in epilepsy.** *Magn Reson Imaging* 1999;17:29–36
15. Kalus P, Buri C, Slotboom J, et al. **Volumetry and diffusion tensor imaging of hippocampal subregions in schizophrenia.** *Neuroreport* 2004;15:867–71
16. Ardekani BA, Bappal A, D'Angelo D, et al. **Brain morphometry using diffusion-weighted magnetic resonance imaging: application to schizophrenia.** *Neuroreport* 2005;16:1455–59
17. Shepherd TM, Thelwall PE, Stanisz GJ, et al. **Chemical fixation alters the water microenvironment in rat cortical brain slices: implications for MRI contrast mechanisms.** *Proc Intl Soc Magn Reson Med* 2005;13:619
18. Shepherd TM, Thelwall PE, King MA, et al. **Cytoarchitectural basis for water diffusion in rat hippocampal slices.** *Proc Intl Soc Magn Reson Med* 2004;12:1231
19. McBain CJ, Traynelis SF, Dingledine R. **Regional variation of extracellular space in the hippocampus.** *Science* 1990;249:674–77
20. Wakana S, Jiang H, Nagae-Poetscher LM, et al. **Fiber tract-based atlas of human white matter anatomy.** *Radiology* 2004;230:77–87
21. Amaral DG, Witter MP. **The three-dimensional organization of the hippocampal formation: a review of anatomical data.** *Neuroscience* 1989; 31:571–91
22. Özarslan E, Vemuri BC, Mareci TH. **Generalized scalar measures for diffusion MRI using trace, variance, and entropy.** *Magn Reson Med* 2005;53:866–76
23. Frank LR. **Anisotropy in high angular resolution diffusion-weighted MRI.** *Magn Reson Med* 2001;45:935–39
24. Tuch DS, Reese TG, Wiegell MR, et al. **High angular resolution diffusion imaging reveals intravoxel white matter fiber heterogeneity.** *Magn Reson Med* 2002;48:577–82
25. Özarslan E, Shepherd TM, Vemuri BC, et al**. Resolution of complex tissue microarchitecture using the diffusion orientation transform (DOT).** *Neuroimage* 2006;31:1086–103. Epub 2006 Mar 20
26. Pierpaoli C, Basser PJ. **Toward a quantitative assessment of diffusion anisotropy.** *Magn Reson Med* 1996;36:893–906
27. Shepherd TM, Flint J, Thelwall PE, et al. **Postmortem interval alters the water relaxation and diffusion properties of nervous tissue: implications for high resolution MRI of human autopsy samples.** *Proc Intl Soc Magn Reson Med* 2006;14:139
28. Seaman WJ. *Postmortem Change in the Rat: A Histologic Characterization*. Ames, Iowa: Iowa State University Press; 1987
29. Burton EC, Nemetz PN. **Medical error and outcomes measures: where have all the autopsies gone?** *MedGenMed* 2000;2:E8
30. Sun SW, Neil JJ, Song SK. **Relative indices of water diffusion anisotropy are equivalent in live and formalin-fixed mouse brains.** *Magn Reson Med* 2003;50:743–48